Journal of Solar Energy Research (JSER)

Journal homepage: www.jser.ut.ac.ir

Enhancing the Performance of a Double-Slope Solar Still Using Thin and Twisted Fins: A Numerical Study

Duraid T. Mahmood[a,*], Ziyad T. Sfaieeh[b]

[a]*Middle Technical university, Polytechnic College of Engineering Specializations-Baghdad, Power mechanics Techniques, Baghdad, Iraq*
[b]*Middle Technical University, Engineering Technical College – Baghdad, Fuel and Energy Techniques Engineering Department, Baghdad, Iraq*

ARTICLE INFO

Article Type:

Research Article

Received:2026.06.21
Accepted in revised form:2026.08.07

Keywords:
Double-slope solar still; Fin geometry; Twisted fins; CFD analysis; Evaporation enhancement; Solar desalination

A B S T R A C T

Water scarcity is a global issue. Solar desalination systems, particularly double-slope solar stills (DSSS), offer an efficient, affordable approach to produce fresh water. This study systematically investigates the influence of fin geometry (thin vs. twisted) and fin number on the thermo-fluid behavior and productivity of DSSS under hot climatic conditions. Using ANSYS Fluent 2019 R1, the mass, momentum, and energy equations were discretised via the finite volume method to examine simultaneous heat, mass, and fluid flow inside the basin. Results show that using fins significantly enhances system performance. At peak time (12:00 PM), productivity improved from 0.8206 L/h (conventional) to 1.4928 L/h for thin fins (81.91% enhancement) and 1.9535 L/h for twisted fins (138.13% enhancement). Efficiency likewise improved from 28.543% to 59.810% and 80.500%, respectively. On a daily basis, productivity and efficiency increased from 3.514 to 8.761 L/m²·day and from 25.87% to 74.97% using 49 twisted fins, representing improvements of 149.32% and 189.68%. Twisted fins exhibit superior performance by enhancing internal mixing, reducing thermal boundary layer thickness, and improving vapor distribution. Ultimately, the best results were obtained with 49 twisted fins, demonstrating that sophisticated geometric modifications are essential to maximize DSSS productivity and efficiency.

1. Introduction

Global water consumption increased substantially over the past century due to population growth, urbanization, and industrial development[1]. Although approximately 70% of the Earth's surface is covered by water, nearly 97% is saline water, whereas only about 3% is freshwater. Of this freshwater, a large proportion is stored in ice caps and groundwater, leaving only a small percentage readily

*Corresponding Author Email:duraid.thamer@mtu.edu.iq

Cite this article: Mahmood,D Thamer and Sfaieeh,Z Tariq. (2026). Enhancing the Performance of a Double-Slope Solar Still Using Thin and Twisted Fins: A Numerical Study. Journal of Solar Energy Research, 11(3), 4021-4035. doi: 10.22059/jser.2026.415805.1759

DOI: 10.22059/jser.2026.415805.1759

accessible for human consumption, as shown in Figure 1 [2]. The limited accessibility of freshwater has therefore intensified the global challenge of water scarcity. This problem can be addressed by converting seawater into freshwater through desalination [3]. However, conventional desalination systems are generally energy-intensive and costly. Therefore, solar desalination represents a cost-effective alternative, particularly in regions with abundant solar radiation. The double-slope solar still (DSSS) was one such system and was found to be more efficient than conventional solar stills. It has two sloping glass covers to enhance the absorption of solar heat and increase the area for condensation. Solar energy is used to evaporate the saline water, and the resulting vapor condenses on the glass covers to produce freshwater [4]. Although many solar desalination systems had been developed, the effects of fin geometry and fin density on the coupled heat- and mass-transfer processes within DSSSs remained poorly understood, especially for twisted fin systems under high solar insolation.

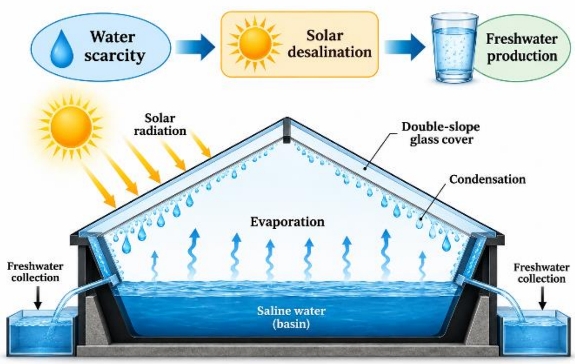

Figure 1. From Global Water Scarcity to Sustainable Desalination: DSSS Concept and Working Principle

Rajaseenivasan & Srithar [5] conducted a combined experimental and theoretical study to enhance the productivity of a single-slope solar still(SSSS) in conditions of Madurai, India (9°56 N, 78°07 E). Their experiment assessed circular and square fin integration, some of which were wick-supported, at depths of water in the basin of 1-4 cm. The results showed that the square-fin configuration integrated with wick material achieved the best performance, which produced a maximum of freshwater of 4.55 L/m²·day and increased the productivity by 45.8 % as compared with the conventional design. Khare et al. [6] used CFD simulations on ANSYS software to determine the thermal and productivity performance of SSSS systems in Jaipur, India (26°13’N, 75°49’E). Their numerical study explored the effects of changing basin depths and absorber surface materials in the context of regional climatic conditions. The optimized system had a maximum freshwater productivity of 5 L/m²·day with an overall thermal efficiency of 32% and the inclusion of mirrors increased system productivity by about 22 % as compared to the traditional design. Moreno et al. [7] numerically evaluated the effect of adding phase change materials (PCMs) to the bottom of the basin into which an SSSS was deployed in Hermosillo, Mexico (29°05′N, 110°57′W) under the conditions of a desert environment. Their CFD analysis compares four PCM variants (RT54 HC, RT62 HC, RT70 HC and RT80 HC) with a thickness of 0.25, 0.5, and 1 cm in winter and summer seasons. Of all the tested conditions, the RT70 HC at a thickness of 0.25 cm produced the best performance, generating approximately 5.42 L/m²·day with a simulation error of less than 1%. Chung & Kim [8] developed a numerical model to evaluate different fin-and-liquid-cooling arrangements for battery thermal management. Their results showed that the optimized design increased the equivalent heat conductance-to-volume ratio by 64%, while the pressure drop increased by only 19%. Moreover, the symmetric arrangement reduced the maximum temperature difference to 5.4 °C and maintained a 38% improvement in the heat conductance-to-volume ratio. These findings highlighted the importance of considering heat-transfer enhancement, temperature uniformity, and pressure-drop penalties simultaneously in finned thermal systems. Hashemian et al [9] conducted thermo-economic and exergo-environmental analyses of a solar–wind-powered multigeneration system for producing power, heating, cooling, hydrogen, and ammonia. The proposed plant achieved energy and exergy efficiencies of 83.65% and 17.97%, respectively, while producing 44.8 MW of power, 123.9 MW of cooling, 20.64 MW of heating, 263.1 kg/h of hydrogen, and 106.48 kg/h of ammonia. The parabolic trough collector accounted for approximately 57% of the total exergy destruction, and an ambient temperature of 35 °C provided the best exergy-environmental performance. Their results emphasized the importance of component-level exergy analysis for identifying the principal sources of thermodynamic irreversibility. Hafs et al. [10] used COMSOL Multiphysics and finite element modelling to study seasonal thermal optimization of SSSS systems in Rabat, Morocco (34°02′N, 6°50′W). The investigated solar stills were equipped with rectangular thermal-storage channels, and several geometrical parameters, including channel number and width, were optimized for different seasonal conditions. The configuration containing five rectangular channels, each 2 cm wide, achieved the best summer performance, with a freshwater productivity of 2.92 L/m²·day, and overall thermal efficiency of 157%. Hameed et al. [11] constructed a three-dimensional numerical model with the help of COMSOL Multiphysics to enhance the area of evaporation in an SSSS situated in Najaf, Iraq (32.0316°N, 44.3219°E). The basin was modified by adding 15 stainless-steel elements in different configurations to maximize the effective evaporation surface area. The optimized design reached a peak freshwater yield of 4.13 L/m²·day and increased basin temperature to 72.9 °C, which confirmed the effectiveness of the expanded evaporation surfaces in enhancing the performance of the system. Aftiss et al. [12] conducted a comparative numerical study in six cities of Morocco to evaluate the SSSS productivity under different seasonal conditions Two scenarios of thermal energy storage were studied: paraffin-wax PCM alone and PCM combined with a storage tan. Their results indicated that the maximum freshwater productivity was recorded in Marrakesh (31.6278°N, 7.9811°W) of 8.6 L/m²·day in the PCM-storage tank setup, whereas the highest energy efficiency of 76.05% was achieved in Agadir (30.4278°N, 9.5981°W). AbdelMeguid et al. [13] investigated the impact of glass cover optical properties on the SSSS desalination performance in Matruh, Egypt (31.35°N, 27.25°E). Their findings showed that increasing the glass thickness from 5 to 20 mm reduced freshwater productivity from 6.6 to 5.2 L/m²·day and decreased thermal efficiency from 31.5% to 24.9%. Thinner glass materials with a lower refractive index and absorption coefficient, such Pyrex or quartz, and seasonally optimal tilt angles were associated with enhanced system performance. Under the optimum summer conditions, the system produced 210 L/m² per month and achieved a daily efficiency of 36%. Abed et al. [14] numerically simulated a pyramid solar still (PSS) under the climatic conditions of Najaf, Iraq, using COMSOL Multiphysics. Their hybrid enhancement approach combined flat reflectors, PCM, and CuO nanoparticles, resulting in a maximum freshwater yield of 8.14 L/m²·day and a 112.34% increase in daily energy efficiency, thereby demonstrating the considerable potential of combined thermal-enhancement strategies. Aftiss et al. [15] introduced a dynamic PCM-layer strategy to increase the productivity of an SSSS in Agadir, Morocco (30.4278°N, 9.5981°W). Their numerical investigation was conducted under representative sunny-day conditions. The dynamic PCM configuration achieved a freshwater productivity of 6.04 L/m²·day, an energy efficiency of 62.11%, and an approximately 23.26% increase in total freshwater production, demonstrating the effectiveness of adaptive thermal storage in advanced solar-desalination systems. Kavasoğullari et al. [16] carried out a two-dimensional numerical study of the effects of the single-fin inclination angle on the melting dynamics and energy storage capacity of phase change materials (PCMs). The researchers simulated a two-dimensional square enclosure filled with RT27 PCM and subjected it to a constant heat flux of 1000 W/m to either the left or right wall, while all the remaining walls were treated as adiabatic. The study compared a finless baseline with enclosures with a single copper fin mounted at inclination angles of 0°, 15°, 30°, 45°, and 60°. Yazdanparast et al. [17]performed a numerical investigation of the melting and solidification phenomena of phase change materials (PCMs) in a finned rectangular enclosure under realistic and time-dependent solar heat flux. The researchers implemented the enthalpy–porosity method in COMSOL Multiphysics to analyse the thermal performance of systems containing a combination of lauric acid and paraffin wax, as well as systems containing only paraffin wax. A comprehensive parametric study was conducted to examine the influence of chamber inclination angles of 15°, 30°, and 45°; fin configurations with no fins, one fin, and three fins; fin lengths of 1 and 2 cm; and chamber thicknesses of 2.5 and 5 cm (1 cm and 2 cm) and chamber thickness (2.5 cm and 5 cm). Despite the considerable progress reported in solar desalination and the application of various thermal-enhancement techniques, several important research gaps remained unresolved. In particular, limited literature compared the thermo-fluid performance of complex fin geometries with that of conventional straight fins in DSSS systems. The novelty of the present work lies in providing a detailed CFD-based quantitative comparison between thin- and twisted-fin configurations in a DSSS with particular emphasis on the coupled thermo-fluid interactions and vapor-transport mechanisms. This study aimed to examine the effects of fin geometry, thin and twisted, and fin number on the thermo-fluid performance of a DSSS operated under hot-climate conditions. The objective was to enhance heat and mass transfer within the basin, thereby increasing the evaporation rate, freshwater productivity, and thermal efficiency, and to identify the fin configuration that maximized the overall system performance.

2. Physical Description of the Model

A DSSS with the geometrical dimensions shown in Figure 2 was modelled in the present study. The basin base measured 1000 × 1000 mm, providing a large surface area for solar-energy absorption and water evaporation. The effective length of the still was 998 mm, while each inclined glass cover measured 589 mm in length and served as a condensation surface. The still's rear height is approximately 412 mm, corresponding to the inclination angle of 32°.

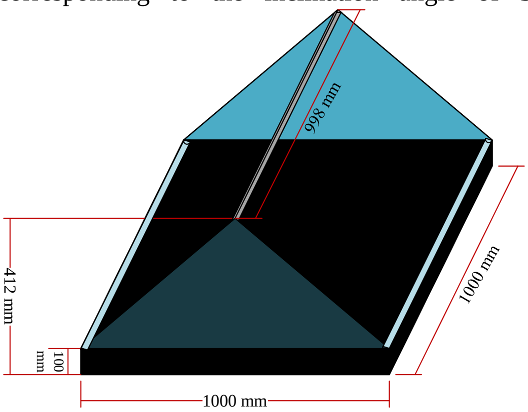

Figure 2. Dimensions of the DSSS model

The basin was equipped with two fin geometries: thin straight fins and twisted fins. In all investigated cases, the fins had identical dimensions: a length of 50 mm, a thickness of 10 mm, and a height of 30 mm. For the thin straight-fin configurations, three copper-fin arrangements containing 36, 42, and 49 fins were investigated. The corresponding fin spacings were 150 × 150 mm, 150 × 125 mm, and 125 × 125 mm, respectively, as illustrated in Figure 3.

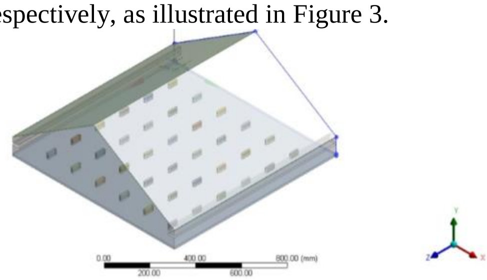

a) 36 thin fins

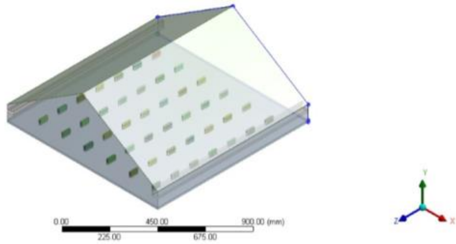

b) 42 thin fins

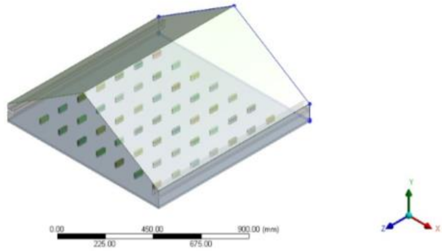

c) 49 thin fins

Figure 3. Configurations of a) 36, b) 42, and c) 49 thin fins

For the copper twisted fins, the same fin numbers (36, 42 and 49 fins) were used with a twist of 0.25 turn (quarter turn) along the fin length, but with the same spacing patterns, as shown in Figure 4.

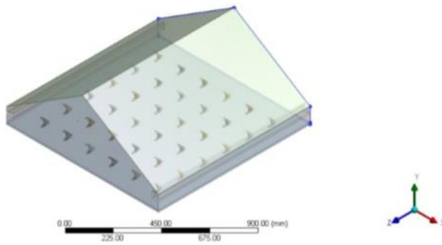

a) 36 twisted fins

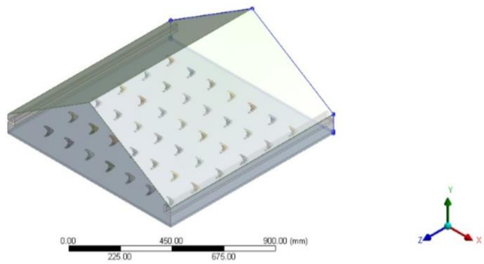

b) 42 twisted fins

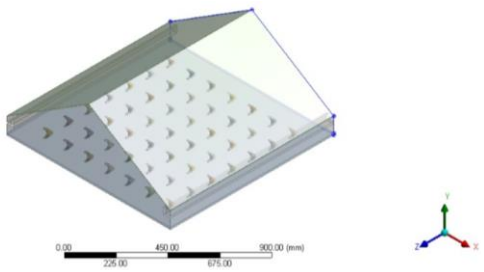

c) 49 twisted fins

Figure 4. Twisted-fin configurations: (a) 36 fins, (b) 42 fins, and (c) 49 fins

3. Mathematical Model

The numerical model of the DSSS was based on the conservation equations of mass, momentum, and energy. These equations represent the thermo-fluid dynamics inside the still, such as natural convection, heat transfer, evaporation and vapor flow. The governing equations employed in the present study were formulated as follows. The continuity equation, which expressed mass conservation within the computational domain, was written as follows [18]:

$$\frac{\partial \rho}{\partial t} + \rho \nabla \cdot \vec{v} = 0 \quad (1)$$

Fluid motion resulting from pressure, viscous, and body forces was described by the momentum equation [19]:

$$\left(\frac{\partial \vec{v}}{\partial t} + \vec{v} \cdot \nabla \vec{v} \right) = -\frac{\nabla P}{\rho} + \nu \nabla^2 \vec{v} + \vec{f} \quad (2)$$

Heat transfer within the fluid domain was described by the energy equation [19]:

$$\rho C_p \left(\frac{\partial T}{\partial t} + \vec{v} \cdot \nabla T \right) = K \nabla^2 T + \phi \quad (3)$$

where ρ, $\vec{v}$, P, ν, T, C_p, K, and ϕrepresent density, velocity vector, pressure, kinematic viscosity, temperature, specific heat, thermal conductivity, and viscous dissipation, respectively.

Convective heat transfer between the saline water surface and the glass cover is driven by the temperature difference between them. The convective heat transfer rate is expressed as [20]:

$$Q_{cw} = h_{cw} A_w \left(T_w - T_g \right) \quad (4)$$

where Q_{cw} is the convective heat transfer rate, $h_{cw}$is the convective heat transfer coefficient, $A_w$is the water surface area, $T_w$is the water temperature, and $T_g$is the glass temperature. The convective heat transfer coefficient is related to the Nusselt number, and the Grashof and Prandtl numbers are given by [21]:

$$Nu = \frac{h_{cw} d}{K} = C(Gr \times Pr)^n \quad (5)$$

$$h_{cw} = \frac{CK}{d} (Gr \times Pr)^n \quad (6)$$

$$Gr = \frac{g \beta d^3 \rho_v^2 \Delta T}{\mu^2} \quad (7)$$

$$Pr = \frac{\mu C_v}{K} \quad (8)$$

As discussed in [22], the temperature dependent thermo-physical properties of water vapor were obtained and can be expressed as:

$$K = 0.0244 + 0.7673 \times 10^{-4} \times T_g \quad (9)$$

$$\rho_v = \frac{353.44}{\left(T_v + 273.15 \right)} \quad (10)$$

$$\beta = \frac{1}{\left(T_v + 273.15 \right)} \quad (11)$$

$$\mu = 1.718 \times 10^{-5} + 4.620 \times 10^{-8} \times T_v \quad (12)$$

$$C_v = 0.1434 \times T_v + 1.101 \times 10^{-4} \times T_v - 6.7581 \times 10^{-8} \times T_v^3 + 999.2 \quad (13)$$

$$\mathrm{h_{fg}} = 2.4935 \times 10^6 \begin{pmatrix} 1 - 9.4779 \times 10^{-4}\ \mathrm{T_v} \\ + 1.3132 \times 10^{-7}\ \mathrm{T_v^2} \\ - 4.7974 \times 10^{-9}\ \mathrm{T_v^3} \end{pmatrix} \quad (14)$$

Physically, an increase in the water–glass temperature difference enhances buoyancy-driven flow. This leads to stronger natural convection and improved heat and mass transfer within the enclosure. The evaporative heat transfer coefficient is given by [22]:

$$q_{ew} = h_{ew} \left(T_w - T_g \right) \quad (15)$$

$$h_{ew} = 16.23 \times 10^{-3} h_{cw} \frac{(P_w - P_g)}{(T_w - T_g)} \quad (16)$$

where $P_w$and P_g are the vapour pressures at the water surface and glass cover, respectively. The hourly distilled water production and the vapour pressures are calculated as [22]:

$$m_{ew} = \frac{q_{ew} A_w t_{int}}{h_{fg}} \quad (17)$$

$$P_w = \exp(25.317 - \frac{5144}{T_w + 273.15}) \quad (18)$$

$$P_g = \exp(25.317 - \frac{5144}{T_g + 273.15}) \quad (19)$$

where m_{ew} is the mass of the evaporated water, t_{int} is the time step, and h_{fg} is the latent heat of vaporisation. Accordingly, the enhancement in evaporation can be described through the following thermodynamic relationship:

$$T_w \uparrow \Rightarrow \left(P_w - P_g\right) \uparrow \Rightarrow h_{ew} \uparrow \Rightarrow m_{ew} \uparrow \quad (20)$$

The hourly thermal efficiency of the DSSS is given by [23]:

$$\eta_h = \frac{m_{ew} h_{fg}}{I \tau \alpha A_w \times 3600} \quad (21)$$

I is the solar irradiance, $\tau\alpha$ the transmittance-absorptance product and A_w the water surface area. This equation suggests that the thermal efficiency rises with distilled water production:

$m_{ew} \uparrow \Rightarrow \eta_h \uparrow$

In general, the fins increase the effective heat transfer surface and water temperature. Twisted fins further improve the heat transfer by disrupting the flow, thinning the thermal boundary layer, and promoting fluid mixing. As a result, the combined enhancement of heat transfer, vapour pressure difference, and internal circulation results in increased evaporation rate, productivity and thermal efficiency.

3.1. *Meshing of the DSSS simulation model*

An unstructured mesh was used to discretise the computational domain to capture the complex geometry of the basin and fin arrangement, as depicted in Figure 5. A mesh with 2.1 million elements and 453,000 nodes has been developed to achieve adequate resolution, especially around the fin and wall regions. A mesh independence study was performed to verify the accuracy and reliability of the computational results, with the number of elements ranging from 0.8 million to 2.8 million. The influence of mesh size on important variables, such as glass temperature, water temperature, velocity, productivity and thermal efficiency, is shown in Figures (6-10). As can be seen, significant changes occur at lower mesh resolutions; however, at around 2.0-2.2 million elements, variations become less than approximately 2–3%, indicating mesh-independent behaviour. As such, the mesh with around 2.1 million elements was chosen to balance the cost and accuracy of the numerical results.

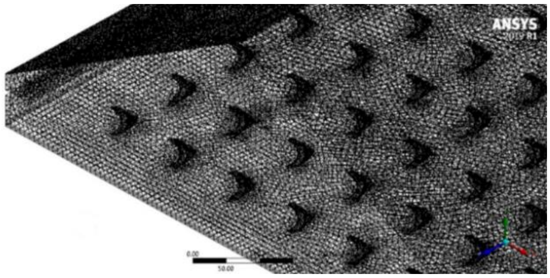

Figure 5. Computational mesh of the solar still model

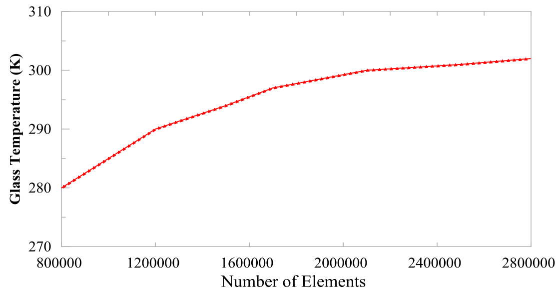

Figure 6. Grid independence study of glass temperature

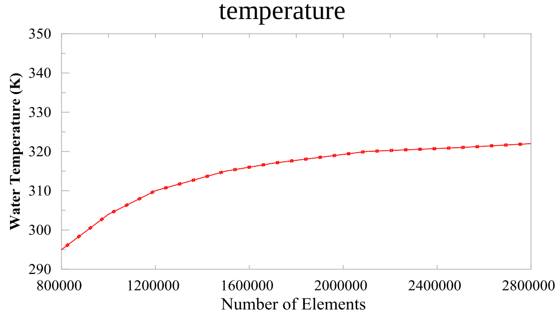

Figure 7. Grid independence study of water temperature

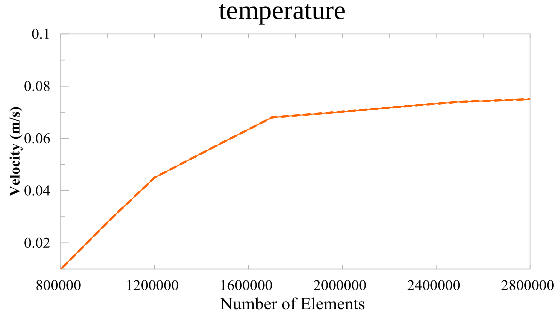

Figure 8. Grid independence study of Velocity

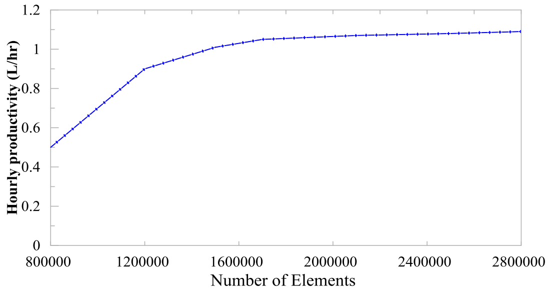

Figure 9. Grid independence study of hourly productivity

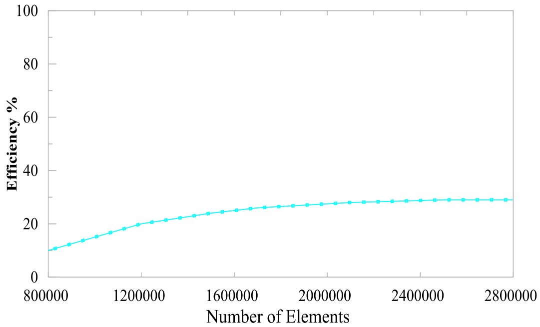

Figure 10. Grid independence study of efficiency

3.2. Initial and boundary conditions

A numerical methodology was developed, with several key input assumptions used to successfully model the complex multi-physics that occurs within the DSSS enclosure. The flow of the fluid inside the basin was assumed to be steady, incompressible and laminar. The assumption of steady laminar flow is physically valid in this realistic situation since the fluid is moving only by natural convection, and the calculated Rayleigh numbers are always small enough for this flow to stay in the laminar range for the specified temperature differences and enclosure sizes. The buoyancy-driven flow was simulated using the Boussinesq approximation, since the variations in the density of the fluid are confined and are mostly due to the differences in temperature between the hot basin and the cold glass cover. In addition, the thermophysical properties of saline water and vapor mixture were determined to be temperature dependent to provide high fidelity in mass transfer modelling and evaporation. The Surface-to-Surface (S2S) radiation model has been used to account for the radiation between the water surface and the inner glass cover with standard emissivity values for copper fins, saline water and glass surfaces. A single-basin DSSS was simulated in ANSYS Fluent under realistic operating conditions.

The initial conditions assumed that at t=0, the temperatures of the saline water, glass cover and absorber plate were at ambient temperature:

$$T_w(x,y,z,0) = T_g(x,y,z,0) = T_p(x,y,z,0) = T_a = 25^{\circ}C, \vec{v}(x,y,z,0) = 0$$

This guarantees a uniform initial thermal condition and zero initial flow. Insulated surfaces were assumed to be adiabatic to minimize heat loss. The absorber plate and glass cover were exposed to convective and radiative heat transfer to simulate the heat exchange with the environment. The boundary conditions are summarised in Table 1.

Table 1: Boundary Conditions for DSSS Model

Surface	**Boundary Condition**
Back side (insulated)	Adiabatic ($q = 0$)
Bottom side (insulated)	Adiabatic ($q = 0$)
Lateral sides (insulated)	Adiabatic ($q = 0$)
Absorber plate	Convection and radiation
Glass cover	Convection and radiation

In the numerical simulations, the mass, momentum and energy conservation equations were solved using the finite volume method (FVM). The second-order upwind scheme was applied to enhance the accuracy of the solution, and the SIMPLE algorithm was applied to couple the pressure and velocity. To achieve convergence and stability, the convergence criteria of 10^{-6} for the energy equation and 10^{-4} for the continuity and momentum equations, respectively, were used. The flow inside the solar still was assumed to be steady, incompressible and laminar, as it is in natural convection. This is also evident from the Rayleigh number, which is in the laminar range for natural convection inside the enclosure. A 3D model was considered, but the heat and mass transfer are primarily driven by buoyancy forces, which are captured in the 3D model. The properties of water vapour were temperature-dependent for better accuracy. In addition, the radiative heat transfer inside the enclosure was modelled by the surface-to-surface (S2S) radiation model to consider the radiation between the water surface and the glass cover.

4. Validation results

The accuracy and validity of the current CFD model were verified through a validation process, which involved comparing the current model to published experimental and numerical work. The current CFD model was validated against the findings of Agrawal & Singh [24], who studied a modified single-slope solar still under similar climatic conditions in Iraq.

The validation was conducted on the basis of the yield of fresh water and the basin water temperature. The present model predicted a maximum yield of 3.514 kg/m²·day for the conventional case, which is in reasonable agreement with the reported value of approximately 2 kg/m²·day in [24], considering differences in geometry and operating conditions. The deviation between the present model and the reference study is within an acceptable range (approximately 15–20%), as illustrated in Figure 11.

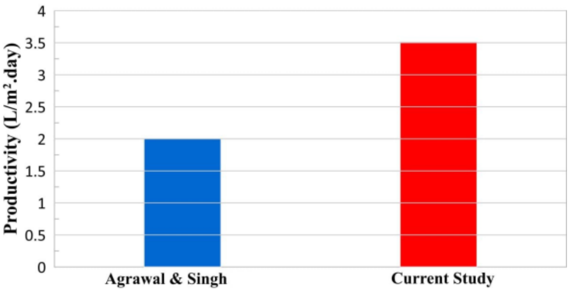

Figure 11. Comparison of freshwater productivity with the reference study

5. Results and Discussion

Figures 12-15 compare the temperature, pressure, velocity and water vapour mass fraction distributions between the original and modified configurations. The findings demonstrate that the addition of fins has a profound effect on the thermo-fluid characteristics within the basin. Thin fins raise the temperature because of the increased heat transfer area and twisted fins perform better because of better mixing and temperature uniformity. From a fluid dynamics perspective, the use of fins leads to higher pressure gradients and velocity distributions, which indicate better mixing. Twisted fins in particular, generate more complex flow patterns and local velocities than thin fins with the same number of fins, due to the increased flow disturbance. This improved flow leads to better mass transfer. The mass fraction of water vapour is more uniform and higher in the finned cases, especially for twisted fins. This implies better evaporation and vapour mixing in the enclosure. Therefore, increasing the number of fins increases the temperature and flow intensities, while twisted fins increase uniformity and mixing. The 49-twisted-fin configuration is the best performing case, with the optimal interaction between heat, flow and mass transfer, and therefore maximum evaporation rate and productivity. This trend illustrates the interaction between heat, flow and mass transfer mechanisms in the DSSS. Figures 16–17 show the hourly productivity and thermal efficiency of the DSSS for the conventional system and thin and twisted fins with different numbers of fins. The diurnal variation of both parameters is similar, with values increasing from 08:00 AM, reaching a maximum at 12:00 PM, and then decreasing until 16:00 PM, in line with the trend of solar irradiance. In the conventional system, the peak productivity and thermal efficiency at 12:00PM are 0.8206 L/h and 28.543%, respectively. The addition of thin fins significantly enhances the performance. The peak productivity increases to 1.0787, 1.2819, and 1.4928 L/h for 36, 42, and 49 fins, corresponding to improvements of 31.46%, 56.22%, and 81.91%, respectively. In parallel, the thermal efficiency reaches 43.379%, 51.472%, and 59.810%, with corresponding increases of 51.98%, 80.33%, and 109.56%. A greater improvement is observed with twisted fins, where the productivity increases to 1.6580, 1.8488, and 1.9535 L/h, or 101.95%, 125.34% and 138.13% for 36, 42, and 49 fins, respectively. Similarly, the thermal efficiency increases to 68.808%, 76.479%, and 80.500%, representing improvements of 141.07%, 168.02%, and 182.05%. It is also noted that productivity and efficiency improve with an increase in the number of fins for both geometries. Figure 18 shows the comparison of daily productivity and solar still efficiency for the DSSS with conventional, thin fin, and twisted fin. The findings show that productivity and efficiency increase with the use of fins and with the number of fins. The productivity and efficiency of the conventional system are 3.514 L/m²·day and 25.87%, respectively. The use of thin fins improves the system performance, with productivity reaching 4.404, 5.140, and 5.935 L/m²·day for 36, 42, and 49 fins, respectively (25.33%, 46.28%, and 68.86% increase, respectively). Similarly, the efficiency rises to 38.05%, 44.87%, and 51.90%, with corresponding increases of 47.06%, 73.38%, and 100.62%. A much greater improvement is observed with twisted fins, where the productivity increases to 7.306, 8.203, and 8.761 L/m²·day for 36, 42, and 49 fins, respectively. This corresponds to an increase of 107.90%, 133.40%, and 149.32% over the conventional system. In parallel, the thermal efficiency increases to 63.04%, 70.11%, and 74.97%, representing improvements of 143.64%, 170.96%, and 189.68%, respectively. Also, the research demonstrates twisted fins outperform thin fins in all cases. For example, at 49 fins, productivity increases from 5.935 to 8.761 L/m²·day, and efficiency increases from 51.90% to 74.97%, which means that there are further increases of 47.61% and 44.45% in productivity and efficiency, respectively. This improvement is a result of the combined effects of heat transfer area and fluid flow. Twisted fins enhance internal flow circulation by inducing secondary flow structures, which improve thermal mixing and reduce temperature gradients within the basin. This leads to an increase in evaporation and hence productivity and efficiency. Overall, the twisted fin configuration with 49 fins has the highest productivity and efficiency, suggesting that complex geometric modification is an important factor in improving DSSS performance.

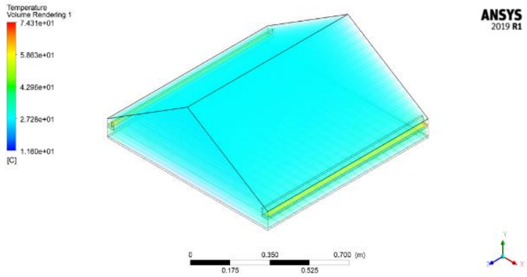

a) Temperature without.

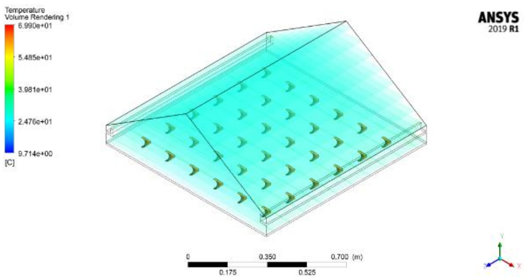

b) Temperature with 36 twisted fins.

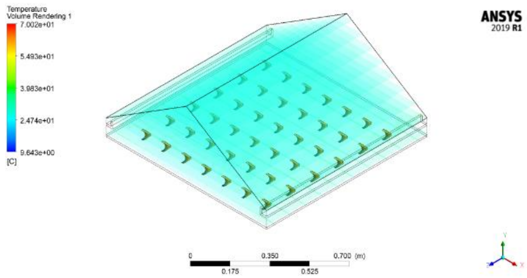

c) Temperature with 42 twisted fins.

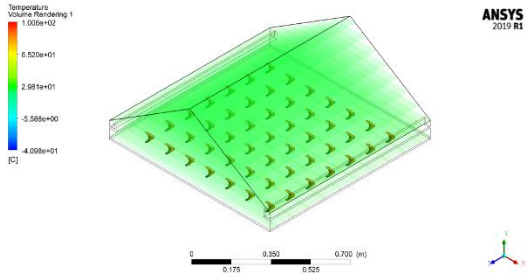

d) Temperature with 49 twisted fins

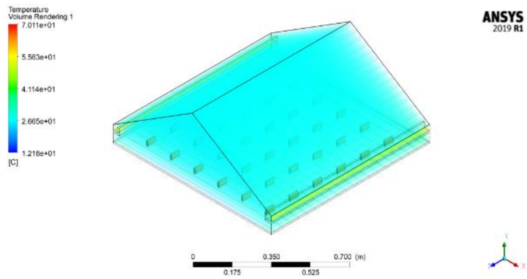

e) Temperature with 36 thin fins.

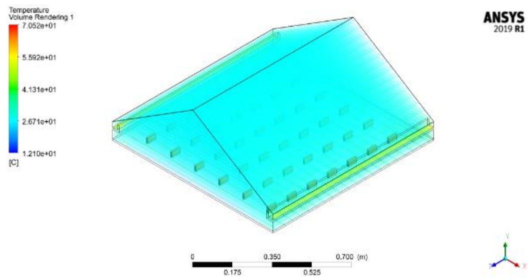

f) Temperature with 42 thin fins.

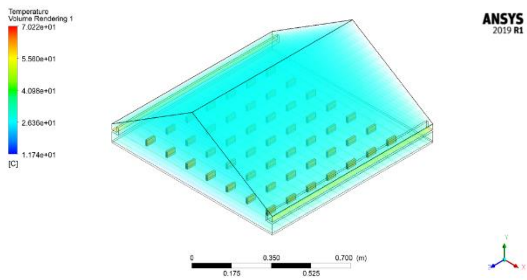

g) Temperature with 49 thin fins.

Figure 12. Contours of temperature for different fin numbers and shapes: (a) Conventional basin without fins, (b) 36 thin fins, (c) 42 thin fins, (d) 49 thin fins, (e) 36 twisted fins, (f) 42 twisted fins, and (g) 49 twisted fins

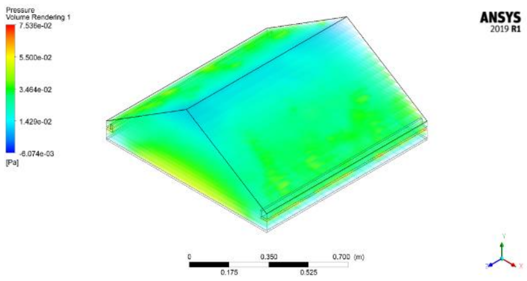

a) Pressure without.

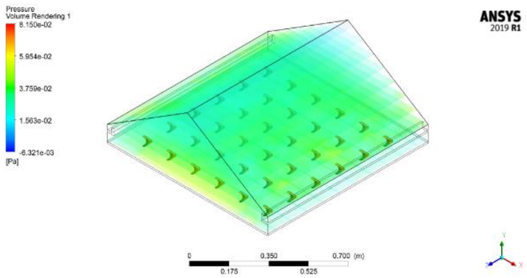

b) Pressure with 36 twisted fins.

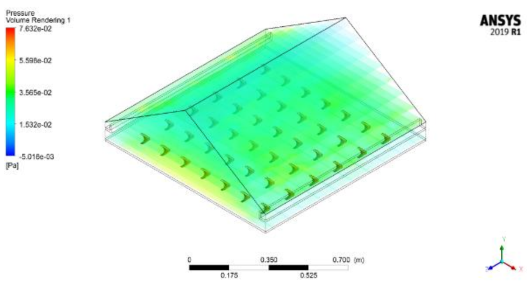

c) Pressure with 42 twisted fins.

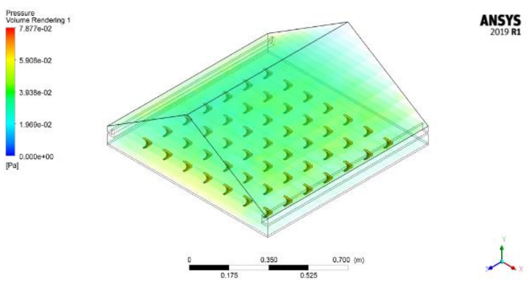

d) Pressure with 49 twisted fins.

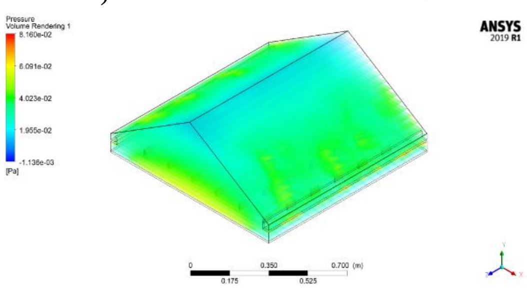

e) Pressure with 36 thin fins.

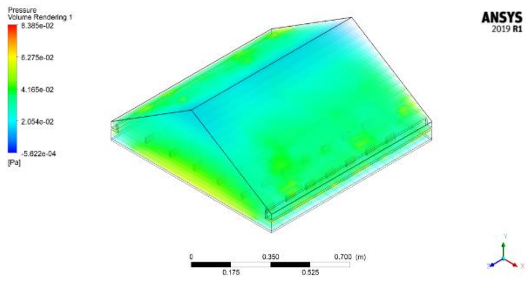

f) Pressure with 42 thin fins.

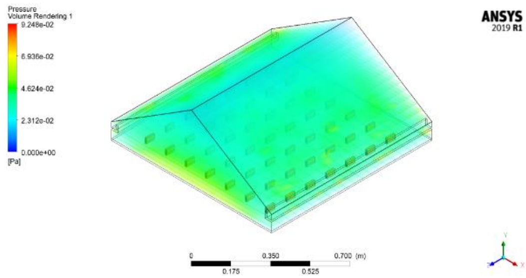

g) Pressure with 49 thin fins.

Figure 13. Pressure contours illustrating the effect of fin design on internal flow: (a) Conventional basin without fins, (b) 36 thin fins, (c) 42 thin fins, (d) 49 thin fins, (e) 36 twisted fins, (f) 42 twisted fins, and (g) 49 twisted fins

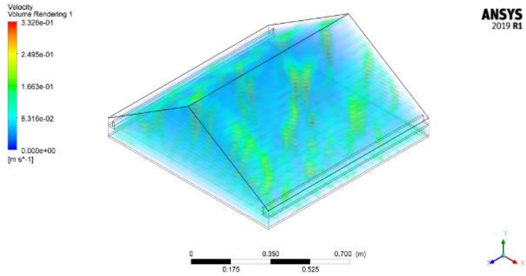

a) Velocity without.

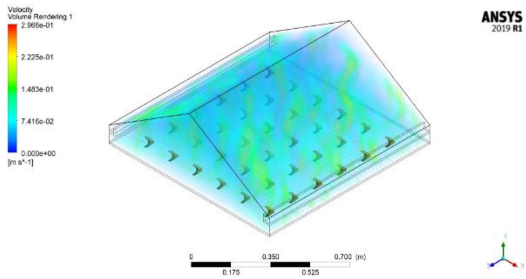

b) Velocity with 36 twisted fins.

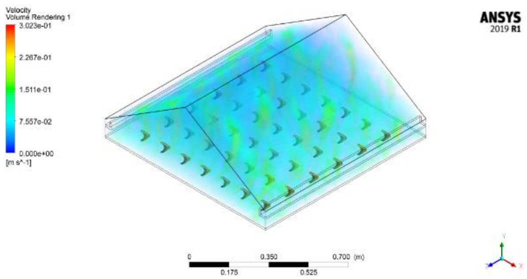

c) Velocity with 42 twisted fins.

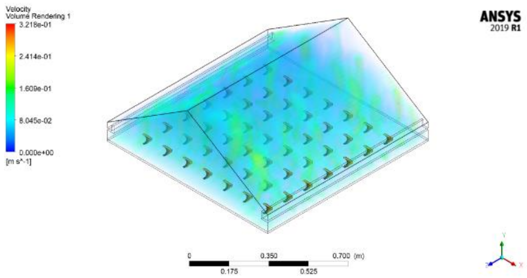

d) Velocity with 49 twisted fins.

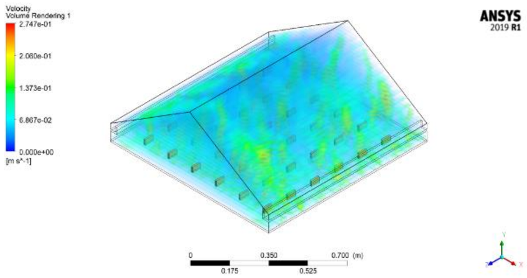

e) Velocity with 36 thin fins.

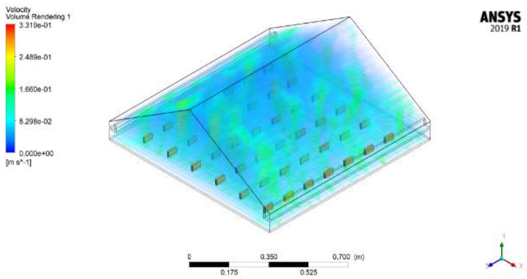

f) Velocity with 42 thin fins

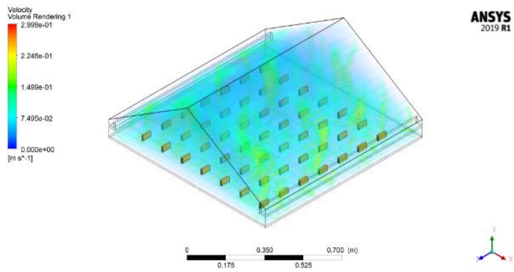

g) Velocity with 49 thin fins.

Figure 14. Velocity contours demonstrating flow structure changes resulting from fin geometry: (a) Conventional basin without fins, (b) 36 thin fins, (c) 42 thin fins, (d) 49 thin fins, (e) 36 twisted fins, (f) 42 twisted fins, and (g) 49 twisted fins

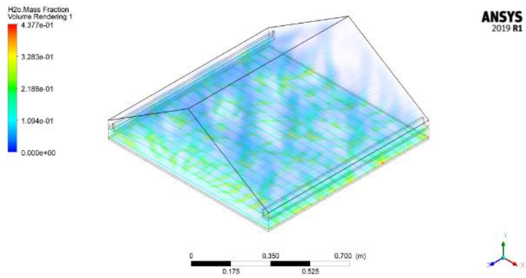

a) H_2O.Mass Fraction without.

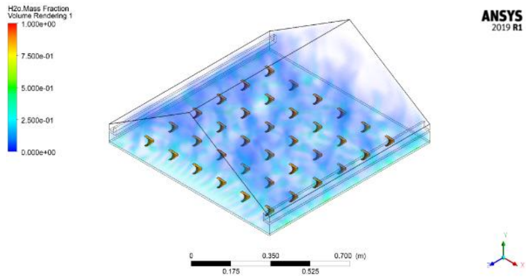

b) H_2O.Mass Fraction with 36 twisted fins.

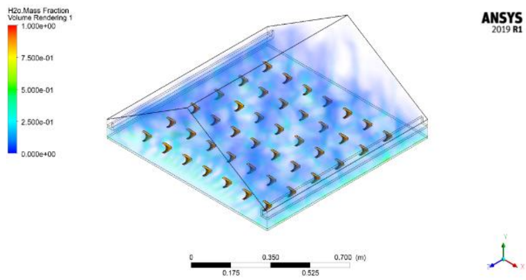

c) H_2O.Mass Fraction with 42 twisted fins.

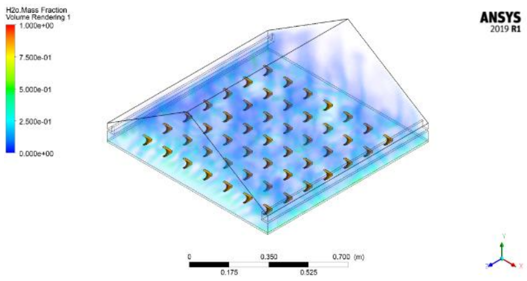

d) H_2O.Mass Fraction with 49 twisted fins.

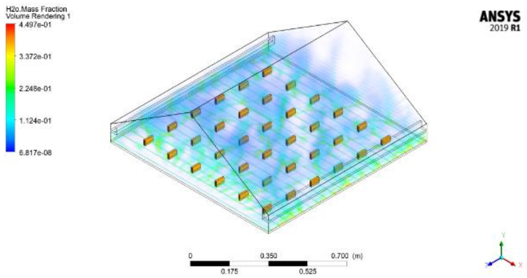

e) H_2O.Mass Fraction with 36 thin fins.

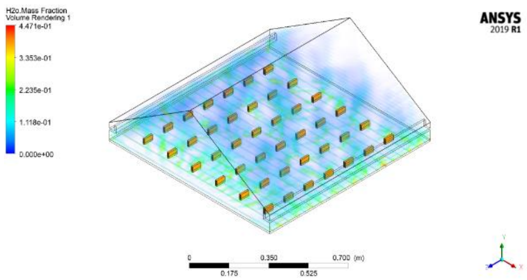

f) H_2O.Mass Fraction with 42 thin fins.

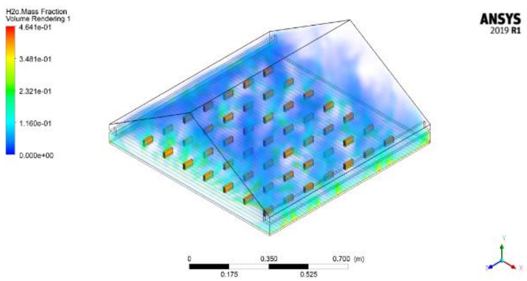

g) H_2O.Mass Fraction with 49 thin fins.

Figure 15. H2O Mass Fraction distribution indicating vapor concentration: (a) Conventional basin without fins, (b) 36 thin fins, (c) 42 thin fins, (d) 49 thin fins, (e) 36 twisted fins, (f) 42 twisted fins, and (g) 49 twisted fins

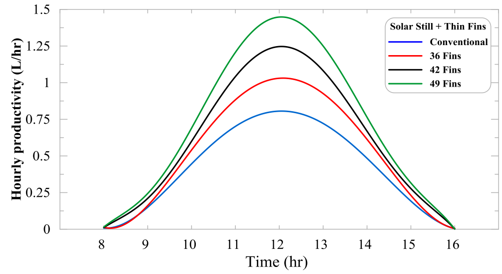

a) Thin fins

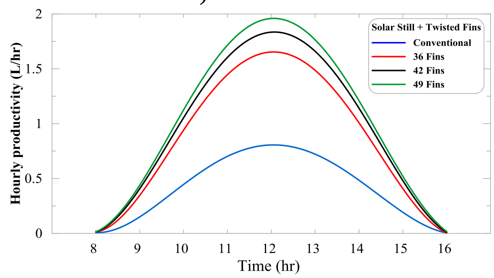

b) Twisted fins

Figure 16. Hourly Productivity of DSSS with a) Thin Fins, b) Twisted Fins with Different Fin Numbers

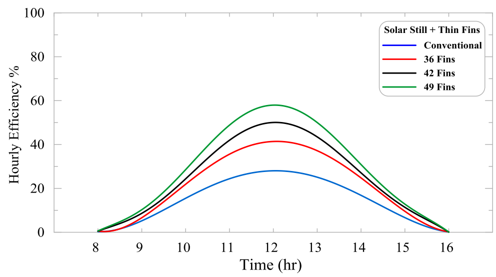

a) Thin fins

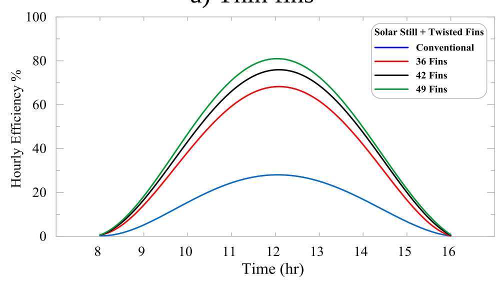

b) Twisted fins

Figure 17. Hourly Thermal Efficiency of DSSS with a) Thin Fins, b) Twisted Fins

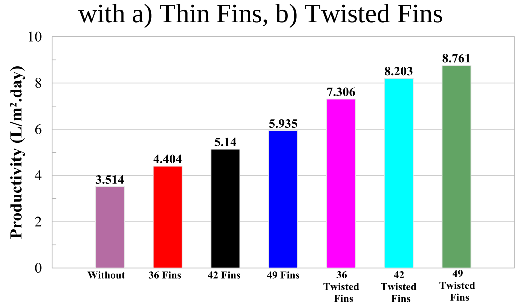

a) Daily Productivity

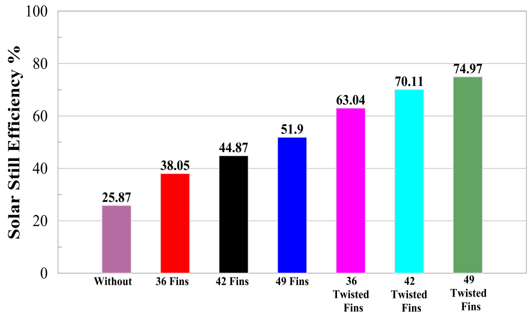

b) Thermal Efficiency.

Figure 18. DSSS a) Daily Productivity, b) Thermal Efficiency for Conventional, Thin and Twisted Fin Configurations

6. Conclusion

ANSYS Fluent 2019 R1 was used to perform a numerical study on the performance of a DSSS in Baghdad, Iraq, in June. The findings show that the use of fins has a positive impact on heat, fluid, and mass transfer inside the basin compared to the conventional case.

1- At the peak time (12:00 PM), the productivity improved from 0.8206 to 1.4928 L/h using thin fins (81.91% enhancement) and to 1.9535 L/h using twisted fins (138.13% enhancement).
2- The thermal efficiency increased from 28.543% (conventional) to 59.810% (thin fins) and 80.500% (twisted fins), with improvements of 109.56% and 182.05%, respectively.
3- Over a day, the productivity improved from 3.514 to 8.761 L/m²·day, and the efficiency improved from 25.87% to 74.97% using 49 twisted fins, which corresponds to 149.32% and 189.68% enhancements, respectively.
4- Performance improved with increasing fin numbers (36-49) for both thin and twisted fins, but twisted fins performed better in all cases.
5- The improvement is due to the combined effects of an increase in heat transfer area, enhancement of internal mixing, and a decrease in the thickness of the thermal boundary layer, which lead to an increase in the evaporation rate and an improvement in vapor transport.
6- CFD analysis showed that twisted fins result in more uniform temperature, velocity, and vapor concentration distributions than thin fins.
7- The best performance was obtained with 49 twisted fins, demonstrating that innovative geometric modification is an important aspect of improving DSSS productivity and efficiency.

These findings provide valuable insights for the design and optimisation of high-performance solar desalination systems, particularly in arid regions with high solar irradiance.

7. Limitation and Future Work

The numerical investigation presented in this paper offers complete understanding of the thermo-fluid behaviour of a DSSS with twisted fins; however, some limitations are to be noted. The steady laminar flow assumption is made for the present computational model. While the assumption of a steady-state is valid for the internal Rayleigh numbers used in this study, it may not be a good approximation for transient turbulent effects that may occur from sudden wind gusts in the environment or from rapid changes in solar insolation under the varying environmental flow conditions of a dynamic real application. Moreover, the results are preliminary and are only theoretically and numerically validated. Future studies will be directed towards the fabrication of a physical prototype of the optimized 49 twisted fin DSSS configuration, with the objective of performing experimental validation with a high level of rigor for the specific configuration under variable and realistic climatic conditions. Further, future studies could focus on synergistically combining these optimized twisted fins with thermal energy storage mediums such as Phase Change Materials (PCMs) or nanofluids for additional improvement of the overnight freshwater generation and basin water capacity.

Nomenclature

Symbol	Description	Unit
A_w	Water surface area	m²
Cp	Specific heat capacity	J/kg·K
Gr	Grashof number	—
h_{cw}	Convective heat transfer coefficient	W/m²·K
h_{ew}	Evaporative heat transfer coefficient	W/m²·K

h_{fg}	Latent heat of vaporisation	J/kg
I	Solar irradiance	W/m²
K	Thermal conductivity	W/m·K
m_{ew}	Evaporated water mass	kg
Nu	Nusselt number	—
P	Pressure	Pa
P_w	Vapour pressure at the water surface	Pa
P_g	Vapour pressure at the glass cover	Pa
Pr	Prandtl number	—
Q_{cw}	Convective heat transfer rate	W
q_{ew}	Evaporative heat flux	W/m²
T	Temperature	K
T_w	Water temperature	K
T_g	Glass temperature	K
T_a	Ambient temperature	K
V	Velocity vector	m/s
β	Thermal expansion coefficient	1/K
η	Thermal efficiency	%
μ	Dynamic viscosity	kg/m·s
ν	Kinematic viscosity	m²/s
ρ	Density	kg/m³
φ	Viscous dissipation	W/m³
DSSS	Double-slope solar still	
CFD	Computational fluid dynamics	
FVM	Finite volume method	
S2S	Surface-to-surface radiation model	

References

[1] Dhivagar, R., Suraparaju, S. K., Jidhesh, P., & Kim, S. C. (2025). Integration of solar photovoltaic panel and A46 phase change material in double-slope solar still: A progressive approach for performance enhancement. *Separation and Purification Technology, 374*, 133754. https://doi.org/10.1016/j.seppur.2025.133754

[2] Saha, S., Sarker, M. R. I., Kader, M. A., Ahmed, M. M., Tuly, S. S., & Mustafi, N. N. (2024). Development of a vacuum double-slope solar still for enhanced freshwater productivity. *Solar Energy, 270*, 112385. https://doi.org/10.1016/j.solener.2024.112385

[3] Ghriss, O., Makki, N., Dhaoui, S., Abdel-Aziz, M. M., Bouabidi, A., & Attia, M. E. H. (2025). Experimental assessment of square fin number variation on energy and exergy performance in double-slope solar stills under Tunisia weather conditions. *International Communications in Heat and Mass Transfer, 162*, 108660. https://doi.org/10.1016/j.icheatmasstransfer.2025.108660

[4] Ghazy, A. (2023). Theoretical study of a double-slope solar still with solar air heater condenser. *International Journal of Renewable Energy Development, 12*(6), 977–986. https://doi.org/10.14710/ijred.2023.53928

[5] Rajaseenivasan, T., & Srithar, K. (2016). Performance investigation on solar still with circular and square fins in basin with CO_2 mitigation and economic analysis. *Desalination, 380*, 66–74. https://doi.org/10.1016/j.desal.2015.11.025

[6] Khare, V. R., Singh, A. P., Kumar, H., & Khatri, R. (2017). Modelling and performance enhancement of single slope solar still using CFD. *Energy Procedia, 109*, 447–455. https://doi.org/10.1016/j.egypro.2017.03.064

[7] Moreno, S., Álvarez, C., Hinojosa, J. F., & Maytorena, V. M. (2022). Numerical analysis of a solar still with phase change material under the basin. *Journal of Energy Storage, 55*, 105427. https://doi.org/10.1016/j.est.2022.105427

[8] Chung, Y., & Kim, M. S. (2019). Thermal analysis and pack level design of battery thermal management system with liquid cooling for electric vehicles. *Energy Conversion and Management, 196*, 105–116. https://doi.org/10.1016/j.enconman.2019.05.083

[9] Hashemian, N., & Noorpoor, A. (2023). Thermo-eco-environmental investigation of a newly developed solar/wind powered multi-generation plant with hydrogen and ammonia production options. *Journal of Solar Energy Research, 8*(4), 1728–1737. https://doi.org/10.22059/JSER.2024.374028.1388

[10] Hafs, H., Ansari, O., & Bah, A. (2023). Performance evaluation of a production system of solar desalination by using rectangular channels with PCM at different seasons. *Acta Ecologica Sinica, 43*(4), 690–700. https://doi.org/10.1016/j.chnaes.2022.09.001

[11] Hameed, H. G., Diabil, H. A. N., & Al-Moussawi, M. A. (2023). A numerical investigation of the enhancement of single-slope single-basin solar still productivity. *Energy Reports, 9*, 484–500. https://doi.org/10.1016/j.egyr.2022.11.199

[12] Aftiss, R., Najim, M., & Hissouf, M. (2024). Numerical study of PCM-integrated solar still efficiency enhancement. *International Journal of Low-Carbon Technologies, 19*, 443–454. https://doi.org/10.1093/ijlct/ctae004

[13] AbdelMeguid, H., & El Awady, W. M. (2024). Optimising solar still performance through glass cover optical properties: A mathematical modeling and theoretical investigation. *Ain Shams Engineering Journal, 15*(3), 102589. https://doi.org/10.1016/j.asej.2023.102589

[14] Abed, A. F., Alshukri, M. J., & Hachim, D. M. (2024). Improving solar still performance via the integration of nanoparticle-enhanced phase change materials: A novel pyramid-shaped design with a numerical simulation approach. *Journal of Energy Storage, 97*, 112980. https://doi.org/10.1016/j.est.2024.112980

[15] Aftiss, R., Najim, M., Tbatou, T., & Hissouf, M. (2025). Numerical study of conventional solar still integrated dynamic PCM layer. *Desalination, 600*, 118493. https://doi.org/10.1016/j.desal.2024.118493

[16] Kavasoğulları, B., Aktemur, C., & Karagöz, M. E. (2026). Numerical investigation of the effect of fin inclination on melting dynamics and energy storage in a PCM-filled square enclosure. *Journal of Engineering Research, 14*(2), 2097–2117. https://doi.org/10.1016/j.jer.2025.12.021

[17] Yazdanparast, S. A., Setareh, M., & Basirat Tabrizi, H. (2026). Numerical investigation of melting characteristics of fin-assisted single and dual PCM latent heat storage system under time-dependent solar heat flux. *Discover Mechanical Engineering, 5*(1), Article 14. https://doi.org/10.1007/s44245-026-00185-z

[18] Togun, H., Homod, R. Z., Sadeghinezhad, E., & Kazi, S. N. (2023). Navier–Stokes equations and high-resolutions: Advancements in accurate incompressible flow simulations. *Knowledge-Based Engineering and Sciences, 4*(2), 51–59. https://doi.org/10.51526/kbes.2023.4.2.51-59

[19] da Silva Junior, L. G., de Oliveira, J. P. J., Ribeiro, G. B., & Pinto, L. F. (2023). Experimental and numerical analysis of a low-cost solar still. *Eng, 4*(1), 380–403. https://doi.org/10.3390/eng4010023

[20] Gaur, M. K., & Tiwari, G. N. (2010). Optimisation of number of collectors for integrated PV/T hybrid active solar still. *Applied Energy, 87*(5), 1763–1772. https://doi.org/10.1016/j.apenergy.2009.10.019

[21] Kumar, S., & Tiwari, G. N. (1997). Estimation of convective mass transfer in solar distillation systems. *Solar Energy, 57*(6), 459–464. https://doi.org/10.1016/S0038-092X(96)00122-3

[22] Tiwari, G. N., Shukla, S. K., & Singh, I. P. (2003). Computer modeling of passive/active solar stills by using inner glass temperature. *Desalination, 154*(2), 171–185. https://doi.org/10.1016/S0011-9164(03)80018-8

[23] Ghazy, A., & Alrowais, R. (2022). Experimental performance of single-slope basin solar still coupled with a humidification–dehumidification cycle. *Sustainability, 14*(23), 15755. https://doi.org/10.3390/su142315755

[24] Agrawal, R., & Singh, K. D. P. (2022). Experimental investigation and computational modelling of double slope solar still integrated with eutectic phase change material. *Journal of Energy Storage, 52*, 104802. https://doi.org/10.1016/j.est.2022.104802